V. CONCLUSIONS

We have demonstrated a technique for the suppression of ground clutter in log-magnitude SAR images that exploits differences in the asymmetry of the probability densities of natural ground clutter and man-made objects. Using a slightly modified version of Pearson's second coefficient of skewness, we have enhanced target-to-clutter levels by 9 dB in SAR scenes containing buildings and simulated vehicles. The skewness metric has also been applied to the segmentation of man-made objects from background clutter in a CFAR algorithm we call SM-CFAR.

R. J. FOGLER
L. D. HOSTETLER
Sandia National Laboratories
Dept. 9137/MS 0356
P.O. Box 5800
Albuquerque, NM 87185-0356

D. R. HUSH
Electrical and Computer Engineering Dept.
University of New Mexico
Albuquerque, NM 87106

REFERENCES

[1] Ulaby, F. T., and Dobson, M. C. (1989)
Handbook of Radar Scattering Statistics for Terrain.
Norwood, MA: Artech House, 1989, 38–40.

[2] Papoulis, A. (1965)
Probability, Random Variables, and Stochastic Processes.
New York: McGraw-Hill, 1965, 195.

[3] Johnson, N. L., and Kotz, S. (1970)
Continuous Univariate Distributions-1.
New York: Wiley, 1970, 196.

[4] Beyer, W. H. (1991)
CRC Standard Mathematical Tables and Formulae (29th ed.).
Boca Raton, FL: CRC Press, 1991, 474–475.

[5] Patil, G. P., Boswell, M. T., and Ratnaparkhi, M. V. (1984)
Dictionary and Classified Bibliography of Statistical Distributions in Scientific Work.
Fairland, MD: International Cooperative Publishing House, 1984, 39–55.

[6] Goldstein, G. B. (1973)
False-alarm regulation in log-normal and Weibull clutter.
IEEE Transactions on Aerospace and Electronic Systems, **AES-9**, 1 (Jan. 1973), 427–445.

[7] Hansen, V. G. (1973)
Constant false alarm rate processing in search radars.
In *Proceedings of the IEEE International Radar Conference '73,* London, 1973, 325–332.

[8] Trunk, G. V. (1978)
Range resolution of targets using automatic detectors.
IEEE Transactions on Aerospace and Electronic Systems, **AES-14** (Sept. 1978), 750–755.

[9] Rohling, H. (1983)
Radar CFAR thresholding in clutter and multiple target situations.
IEEE Transactions on Aerospace and Electronic Systems, **AES-19**, 4 (July 1983), 608–621.

[10] Ghandi, P. P., and Kassam, S. A. (1988)
Analysis of CFAR processors in nonhomogenous background.
IEEE Transactions on Aerospace and Electronic Systems, **AES-24**, 4 (July 1988), 427–445.

Resolution of an Averaging Paradox in the Analysis of Switched-Mode DC-DC Converters

The validity of an intuitive averaging method for estimating the low-frequency signals in switch-mode systems is rigorously examined. It is shown that the approach may lead to erroneous results because it violates the Nyquist Sampling Theorem, and that the resulting aliasing effects may interfere with the estimate of the low-frequency component of the signal. A procedure is proposed to estimate the expected error.

INTRODUCTION

The most interesting aspect of switched mode systems is often their behavior at frequencies much lower than the switching frequency. Such is the case for applications to dc-dc power conversion, where the terms "average signals", "small signal perturbations", and "low frequency components" have been used almost synonymously to describe the low-frequency responses of switched-mode power converters. These concepts are useful to describe the open- and closed-loop dynamics of pulsewidth modulation (PWM) and other switched-mode power conversion systems. They are very important in practical engineering circuit design since the control signal of the closed-loop system is a *low-frequency component.*

Averaging is a valuable tool for both analysis and design, but one should be aware of the hazards of incorrect application. The proper interpretation and use of averaging methods recently has become a topic of lively debate among several of our colleagues. With this correspondence we hope to call attention to the topic and to invite further discussion.

This work is the result of discussions we had concerning averaged small-signal circuit models for switched-mode dc-dc converters that operate in the discontinuous conduction mode (DCM). The discussions focused on the relevance of the low-frequency component of the voltage across the inductor, and they were motivated by the observation that some models contain the inductor explicitly [1, 2], while others do not [3, 4].

Operation in DCM is characterized by the inductor current of the converter starting from zero at the beginning of a switching period, reaching a peak value, and then returning to zero and remaining

Manuscript received March 19, 1992; revised August 23, 1993.

IEEE Log No. T-AES/30/2/15831.

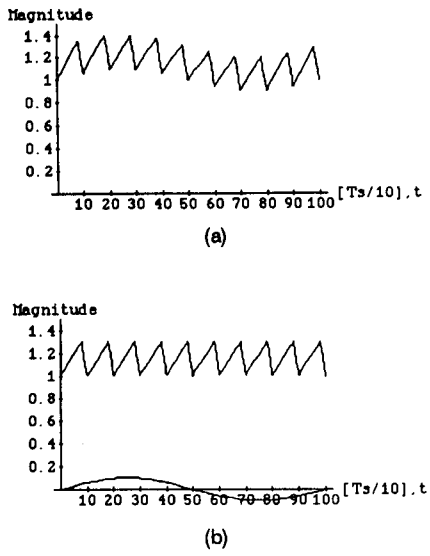

Fig. 1. (a) Typical switch mode. (b) Its components.

there until the beginning of the next period. Since the current of the inductor (and its stored energy) is zero at the beginning and at the end of the period, there is no net change in magnetic flux; hence, the average voltage across the inductor must be zero for that switching period. There is no disagreement that this is true in the steady state, but consider operation in DCM under external low-frequency excitation. If the assertion is true that the average voltage across the inductor is zero for each switching period, how can the voltage of the inductor have a non-zero low frequency component? Consequently, how can the average current in the inductor ever change? Since the average inductor current does in fact change in response to low-frequency external excitations while remaining in DCM, there appears to be a paradox in this averaged description.

THE ONE-SWITCHING CYCLE AVERAGE

A popular concept that is often used to estimate the magnitude of the low-frequency signals, and which was recently applied successfully in a new control technique [5], is the one switching cycle average (OSCA). In this technique, the time-dependent signal is smoothed by replacing it with the average value taken over one switching cycle. For example, consider the switching waveform of Fig. 1(a). This time-dependent signal represents a typical inductor current of a PWM converter operated in the continuous inductor current mode (CCM) in response to a low frequency excitation. The waveform contains a dc component, a low frequency component, and higher frequency components at the switching frequency and its harmonics. Fig. 1(b) shows the low-frequency component, which is normally used to characterize the dynamics of the system, separated from the other components.

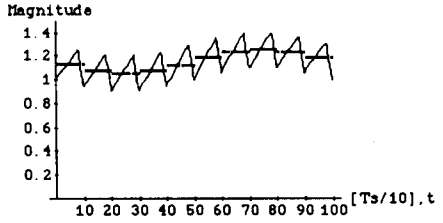

Fig. 2. Output of OSCA on waveform of Fig. 1(a).

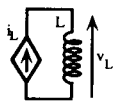

Fig. 3. Benchmark circuit.

The OSCA approach is a simple, intuitive procedure to extract the low-frequency components of switch-mode signals. It is in fact performing the following transformation:

$$s_{av}(kT_s+\tau)=\frac{1}{T_s}\int_{(k-1)T_s+\tau}^{kT_s+\tau} s(\lambda)\,d\lambda \qquad (1)$$

where T_s is the switching period, $s(t)$ is the switching mode signal, s_{av} is the OSCA of the low-frequency component, k is an integer, and $0<\tau<T_s$.

The operation described by (1) can be visualized by considering the illustration of Fig. 2. This representation seems to support the intuitive feeling that the OSCA is a valid approach for estimating the low-frequency component. However, although OSCA may be applied correctly in special cases, it is not valid in general. In fact, as discussed below, application of the OSCA technique may lead not only to errors in the estimate of the magnitude and/or phase of the low-frequency components, but to completely erroneous results. Since averaging techniques are essential for the study and design of switched-mode systems, a rigorous investigation of the validity and limitation of this averaging technique seems to be in order.

THE APPARENT AVERAGING PARADOX

The assertion that there might be a problem with the OSCA technique can be demonstrated with the following example. Consider the network of Fig. 3, which is composed of a current source and an inductor (L). Assume that the current source has the waveform shown in Fig. 4. Since the voltage (v_L) and current (i_L) of an inductor are related by

$$v_L=L\frac{di_L}{dt} \qquad (2)$$

the voltage across the inductor is as shown in Fig. 5.

Consider now two alternative ways to extract the low-frequency component of the voltage across the inductor (v_L). The first approach (Fig. 6(a))

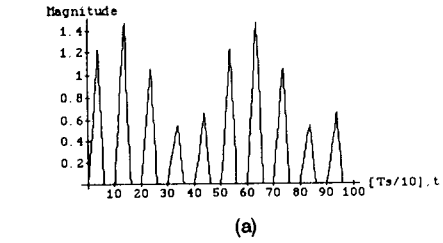

(a)

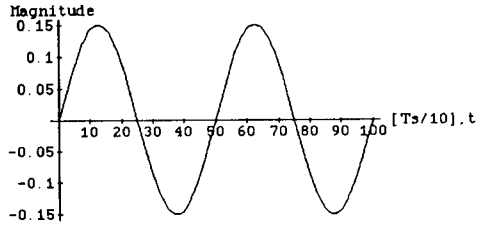

(b)

Fig. 4. (a) Current waveform of source in Fig. 3(a). (b) Its low-frequency component.

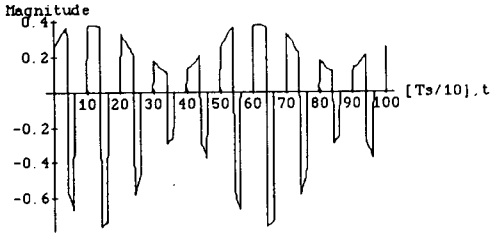

Fig. 5. Steady state voltage across inductor in Fig. 3.

applies a low-pass filter to isolate the low-frequency components. The signal across the inductor obviously includes a low-frequency component which was originally present in the current signal. Denoting the amplitude of the low-frequency component of the current by (I_a) and the frequency by (ω_a), the magnitude of the low-frequency voltage at the output of the low-pass filter is

$$|V_L| = I_a \omega_a L. \tag{3}$$

In the second method of filtering (Fig. 6(b)), the voltage across the inductor is processed by the OSCA approach. From (1) and (2) for $\tau = 0$:

$$v_{L_{av}}(kT_s) = \frac{1}{T_s}\int_{(k-1)T_s}^{kT_s} v_L(\lambda)\,d\lambda = \frac{L}{T_s}\int_{i_L[(k-1)T_s]}^{i_L(kT_s)} di_L$$

$$= \frac{L}{T_s}\{i_L(kT_s) - i_L[(k-1)T_s]\} \tag{4}$$

and since (Fig. 4)

$$i_L[(k-1)T_s] = i_L(kT_s) \tag{5}$$

we find

$$v_{L_{av}}(kT_s) = 0. \tag{6}$$

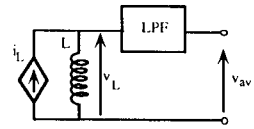

(a)

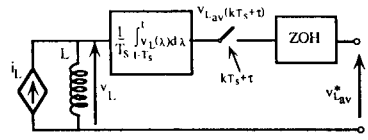

(b)

Fig. 6. Two alternative approaches to extract low-frequency component of voltage across inductor of Fig. 3. (a) By low-pass filter. (b) By OSCA.

The result given by the last equation implies that the output of the OSCA processor (Fig. 6(b)) will be zero all the time.

The contradicting result found in the analysis given above is the source of the apparent averaging paradox noted in the Introduction. This example (and our paradox) demonstrates that the OSCA is not a fail safe technique, and that it may produce grossly erroneous results. It is implicitly assumed, of course, that the frequency domain (i.e., the low-pass filter) method is flawless, and yields the correct value of the low-frequency component of the voltage of the inductor. The analysis that follows shows the OSCA output is in this case an erroneous estimate of the low-frequency component. To gain a better understanding of the origin of the problem, it is addressed in both the time and frequency domains.

TIME DOMAIN ANALYSIS

The OSCA procedure defined by (1) is in fact a sampling operation on the signal $s_{av}(t)$ defined as

$$s_{av}(t) = \frac{1}{T_s}\int_{t-T_s}^{t} s(\lambda)\,d\lambda. \tag{7}$$

This is because the process involves sampling the integral of the signal function under consideration at the discrete times $kT_s + \tau$, which can be shown by substituting $t = kT_s + \tau$ in (7). This presentation clearly shows that the OSCA output is a sampling process of *moving window averaging* (7). That is, the OSCA constitutes an integration over one switching period, a sampling, and a zero-order hold, as shown in Fig. 6(b). In this light, one can easily understand why the OSCA procedure may fail to produce the low-frequency component of the inductor voltage in the mental experiment discussed above. The signal under consideration is shown in Fig. 5, and its continuous time integral is the originating current signal of Fig. 4(a). Since the current is zero at the discrete times kT_s, all the samples are zero; therefore,

the result of the OSCA will be a continuous zero. The same result will be obtained, of course, for any other current waveform that conforms to the relationship:

$$i_L(kT_s + \tau) = i_L[(k-1)T_s + \tau]. \tag{8}$$

An important consequence of this analysis is that the output of the OSCA procedure depends on the phase relationship (represented by τ) between the starting of the switching cycle and the start of the integration. The discussion until now was limited to cases in which $\tau = 0$, i.e., the integration period was from $(k-1)T_s$ to kT_s. For such cases the integration period coincides exactly with the switching period. For the general case, however, the integration period will be from $(k-1)T_s + \tau$ to $kT_s + \tau$. Indeed, examination of the waveforms of Fig. 4 and Fig. 5 clearly shows that the OSCA estimate of the low-frequency component will be a function of the delay (τ). Maximum output will be obtained if the integration will start at the negative transitions of the inductor voltage (Fig. 5), which correspond to the peaks of the current waveform (Fig. 4). Similarly, the OSCA output for the waveform of Fig.1 will also be a function of the delay (τ). This observation causes one to question the validity and accuracy of the low-frequency estimate shown in Fig. 2.

A simple explanation to the inconsistency and erroneous results of the OSCA output is that this procedure violates the Nyquist Sampling Theorem, and hence, it produces aliasing signals. The original signal obviously includes frequencies of $1/T_s$ and above, which are sampled at the switching frequency $f_s = 1/T_s$. This violation may produce spurious (aliasing) signals, which apparently interfere with the averaging process of OSCA. This avenue of thought is further investigated by considering the frequency domain aspect of the problem.

FREQUENCY DOMAIN ANALYSIS

The apparent averaging paradox can be traced to the violation of the Nyquist Sampling Theorem. To investigate further, let us consider the moving window averaging (7) as a filtering process. The operator defined by (7) is a linear and time-invariant system having a transfer function

$$H(j\omega) = \frac{\sin\dfrac{T_s\omega}{2}}{\dfrac{T_s\omega}{2}} \exp\left(j\frac{T_s\omega}{2}\right) \tag{9}$$

that has the absolute value shown in Fig. 7.

Now, let us consider a mathematical model of a typical switch-mode signal as

$$s(t) = \mathcal{L}\left\{m(t)\cdot\sum_l p(t - lT_s)\right\} \tag{10}$$

where $p(t)$ can be any function that exists on the interval $[0,T_s]$, $m(t)$ is a low frequency signal and

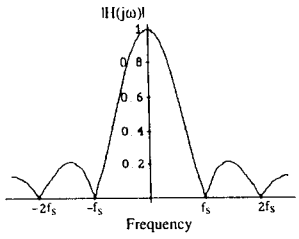

Fig. 7. Absolute value of transfer function of moving window average.

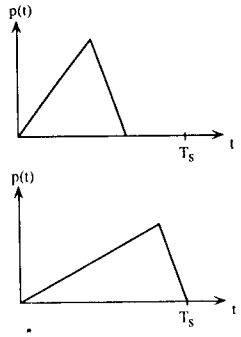

Fig. 8. Examples of $p(t)$ signals.

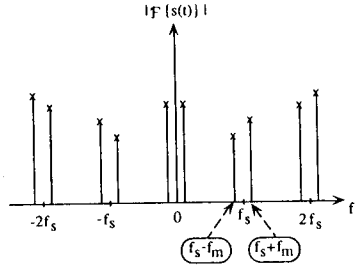

Fig. 9. Absolute value of typical spectrum of switch-mode signal.

$\mathcal{L}\{\cdot\}$ represents a linear operator: a differentiator, for example. Fig. 8 shows two typical examples of $p(t)$, while Fig. 9 shows the absolute value of a typical spectrum of $s(t)$. Reviewing $|H(j\omega)|$ (Fig. 7) and the spectrum of the switch-mode signal shows that the filter defined by (7) *does not reject* the high-frequency components of $s(t)$; therefore, sampling the signal $s_{av}(t)$ at a rate $1/T_s$ may produce aliasing signals exactly at the frequency(ies) of the low-frequency signal $m(t)$. In other words, the Nyquist Sampling Theorem is violated. It is well known that under these conditions the result of the sampling depends on the phase relationship between the sample instants and the sampled signal, i.e., τ in our case.

As a further illustration, in Appendix A the analysis given above is applied to the voltage across the inductor. It is shown that for $\tau = 0$ $v_{L_{av}}(kT_s) = 0$.

ERROR ANALYSIS

The previous section showed that the OSCA procedure can produce errors. The goal now is to make some analytical estimation of the expected error,

and in particular, to find conditions for zero OSCA output.

Denote by $G(j\omega)$ a transfer function of the operator $\mathcal{L}$. Also, suppose that $m(t) = \cos(2\pi f_m t)$. It is easy to see that $\sum_l p(t - lT_s)$ represents a periodic function having period T_s, and therefore,

$$\sum_l p(t - lT_s) = c_0 + \sum_{n=1}^{\infty} c_n \cos(2\pi f_s t + \phi_n). \quad (11)$$

Because of the above, the signal $s(t)$ defined by (10) is a sum of harmonic signals with frequencies f_m, $nf_s \pm f_m$, i.e.:

$$\begin{aligned} s(t) &= C_0 \cos(2\pi f_m t + \varphi_0) \\ &\quad + \frac{1}{2}\sum_{n=1}^{\infty} C_n^{(1)} \cos[2\pi(nf_s - f_m)t + \varphi_n^{(1)}] \\ &\quad + \frac{1}{2}\sum_{n=1}^{\infty} C_n^{(2)} \cos[2\pi(nf_s + f_m)t + \varphi_n^{(2)}] \quad (12) \end{aligned}$$

where

$$C_0 = c_0 |G(j2\pi f_m)| \quad (13)$$

$$C_n^{(1)} = c_n |G[j2\pi(nf_s - f_m)]| \quad (14)$$

$$C_n^{(2)} = c_n |G[j2\pi(nf_s + f_m)]| \quad (15)$$

$$\varphi_0 = \arg\{G(j2\pi f_m)\} \quad (16)$$

$$\varphi_n^{(1)} = \arg\{G[j2\pi(nf_s - f_m)]\} \quad (17)$$

$$\varphi_n^{(2)} = \arg\{G[j2\pi(nf_s + f_m)]\}. \quad (18)$$

Applying the OSCA procedure (7) to $s(t)$ by using (9) we have

$$s_{av}(kT_s + \tau) = C_0 \frac{\sin(\pi T_s f_m)}{\pi T_s f_m} \cos(2\pi f_m k T_s + \eta_0) + \varepsilon(k) \quad (19)$$

where $\eta_0 = 2\pi f_m \tau + \pi f_m T_s + \varphi_0$. $\varepsilon(k)$ denotes the error of the OSCA.

Applying the transfer function $H(j\omega)$ to the last two terms of (12) gives

$$\begin{aligned} \varepsilon(k) &= \frac{\sin(\pi T_s f_m)}{2} \\ &\quad \times \left\{ \sum_{n=1}^{\infty} C_n^{(1)} \frac{(-1)^{n+1}}{\pi(n - T_s f_m)} \cos(2\pi f_m k T_s + \eta_n^{(1)}) \right. \\ &\quad \left. + \sum_{n=1}^{\infty} C_n^{(2)} \frac{(-1)^n}{\pi(n + T_s f_m)} \cos(2\pi f_m k T_s + \eta_n^{(2)}) \right\} \quad (20) \end{aligned}$$

where $\eta_n^{(1)}$ and $\eta_n^{(2)}$ denotes the respective phases.

The error consists of a sum of harmonic sequencies with the same frequency (f_m) but with different phases and amplitudes; therefore, the error $\varepsilon(k)$ itself is a harmonic sequence with the same frequency f_m. Let us define a *normalized error*:

$$\varepsilon_n(k) \stackrel{\text{def}}{=} \frac{\varepsilon(k)}{C_0 \dfrac{\sin(\pi T_s f_m)}{\pi T_s f_m}}. \quad (21)$$

From (20) it follows that:

$$|\varepsilon_n(k)| \le \varepsilon_{\max} = \frac{\frac{1}{2}\sum_{n=1}^{\infty} \left[\dfrac{|C_n^{(1)}|}{n - T_s f_m} + \dfrac{|C_n^{(2)}|}{n + T_s f_m} \right] T_s f_m}{|C_0|}. \quad (22)$$

If $\varepsilon_{\max} = 1$ for all k, and if additionally the phase of $\varepsilon(k)$ equals $\eta_0 + \pi$, then $s_{av}(kT_s + \tau) \equiv 0$.

As an example, consider the case given in Appendix A. We have $c_0 = 1$, $c_1 = -1$ and $c_n = 0$ for $n = 2,3,\ldots$. $G(j\omega) = j\omega$ therefore $C_0 = 2\pi f_m$, $C_1^{(1)} = -2\pi(f_s - f_m)$, $C_1^{(2)} = -2\pi(f_s + f_m)$, $C_n^{(1)} = 0$ and $C_n^{(2)} = 0$ for $n = 2,3,\ldots$. For such data it is easy to check that $\varepsilon_{\max} = 1$. Moreover, for $\tau = 0$ the phase condition is fulfilled, and consequently, $s_{av}(kT_s) \equiv 0$.

DISCUSSION AND CONCLUSIONS

The analysis presented here suggests that OSCA may produce erroneous estimates of the low frequency components of switch-mode converters. The source of the error is traced to the violation of the Nyquist Sampling Theorem inherent in this procedure. The relationship between the time domain and frequency domain aspects of the problem, investigated here, suggest a way to estimate the OSCA errors.

In particular, the analysis shows a weakness in the intuitive cycle-by-cycle approach to finding the average voltage across inductors in switched-mode converters. It leads to the erroneous conclusion that the low-frequency voltage across the inductor in a converter that operates in DCM must be zero.

Another point to consider is the possible effect of the OSCA error on the accuracy of other average models of switched-mode systems. Do any of these suffer from the effects of this error? Much work has been done on the modeling and analysis of dc-dc converter circuits. We list as References only a small sample of the many papers that have contributed to this topic. State space averaging [3, 6, 7] is widely accepted as an analysis tool, and its resulting models for both CCM and DCM have been used extensively. Other methods, which use a more intuitive approach, have since been proposed and demonstrated [4]. More recently, procedures have been presented [1, 2, 8, 9] that extend and generalize the earlier approaches, but only [1 and 2] address DCM.

In the method of state space averaging, the state space equations are written for each topology of the

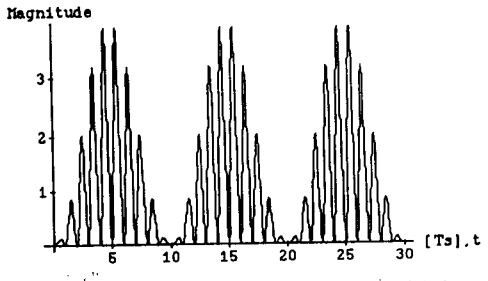

Fig. 10. Switch-mode signal (equation (24)) which is used to demonstrate aliasing problem. Simulation of case $f_m = 0.1 f_s$.

switched system, and the average behavior is estimated by weighting the rate of change over the complete cycle. For example, for continuous mode of operation:

$$\dot{x}_{i_{av}} = \frac{\dot{x}_{i_1}(t_1)t_1 + \dot{x}_{i_2}(t_2)t_2}{T_s} \tag{23}$$

where $\dot{x}_{i_1}$ and $\dot{x}_{i_2}$ are the derivatives of the state variable (i) at the intervals (1) and (2) respectively, and $\dot{x}_{i_{av}}$ is the "average" rate of change. The resulting average differential equation is a continuous function which yields a continuous solution. It would appear that since no sampling is involved, the method is free of the OSCA aliasing error. In the original derivation of the state space averaged models for DCM [3], the requirement for zero instantaneous inductor current was used to eliminate the inductor current as a true state variable, and a different averaged inductor current was substituted. The new quantity is not restricted by sampling, and it can be perturbed as a continuous state variable. Both the PWM switch model [1] and the current injected equivalent circuit approach [4] rely on averaged quantities, but since the defined quantities are implicitly long-term averages, they avoid the sampling difficulties. This hypothesis is substantiated by the excellent agreement between experimental results and the predictions of a general small-signal model recently proposed in [2] for PWM converters in DCM.

There are several different averaged models for dc-dc converters in DCM, and although they are correct within the limits of their originating assumptions, they lead to slightly different results. Could subtleties in applications of the averaging methods explain these differences? Are the differences negligible in practical applications? One switching cycle average, continuous switching cycle average, and running average on one switching cycle period are but few of the possible averages that can be carried out. To avoid confusion and possible error, it is suggested that investigators specify explicitly the type of averaging that is carried out in a given study. It seems that explicit and rigorous definition of the averaging scheme may be very important to our understanding of these models. We hope to encourage further work to resolve questions that remain in the use of averaged models.

APPENDIX A

Consider $p(t) = 1 - \cos((2\pi/T_s)t)$ and $m(t) = 1 - \cos 2\pi f_m t$.[1] Now define the current source:

$$i_L(t) = m(t)\sum_k p(t - kT_s)$$

$$= (1 - \cos 2\pi f_m t)\left[1 - \cos\left(\frac{2\pi}{T_s}t\right)\right]. \tag{24}$$

Fig. 10 shows the current $i_L(t)$.

Applying such current to an inductor of value $L = 1$, will produce a voltage

$$\begin{aligned} v_L(t) &= \frac{d}{dt}\left\{(1 - \cos 2\pi f_m t)\left[1 - \cos\left(\frac{2\pi}{T_s}t\right)\right]\right\} \\ &= 2\pi f_m \sin(2\pi f_m t)[1 - \cos(2\pi f_s t)] \\ &\quad - \cos(2\pi f_m t)\cdot 2\pi f_s \sin(2\pi f_s t) + 2\pi f_s \sin(2\pi f_s t) \\ &= 2\pi f_m \sin(2\pi f_m t) - \pi(f_s + f_m)\sin[2\pi(f_s + f_m)t] \\ &\quad - \pi(f_s - f_m)\sin[2\pi(f_s - f_m)t] + 2\pi f_s \sin(2\pi f_s t) \end{aligned} \tag{25}$$

where the operator $\mathcal{L}\{\cdot\}$ in our case represents a differentiator and $f_s = 1/T_s$.

Applying $v_L(t)$ to the filter $H(j\omega)$ (equation (9)) gives

$$\begin{aligned} v_{L_{av}} &= \frac{2\sin(\pi f_m T_s)}{T_s}\sin(2\pi f_m t + \pi f_m T_s) \\ &\quad - \frac{\sin[\pi(f_s + f_m)T_s]}{T_s}\sin[2\pi(f_s + f_m)t + \pi(f_s + f_m)T_s] \\ &\quad - \frac{\sin[\pi(f_s - f_m)T_s]}{T_s}\sin[2\pi(f_s - f_m)t + \pi(f_s - f_m)T_s]. \end{aligned} \tag{26}$$

Sampling $v_{L_{av}}$ at kT_s and applying elementary trigonometric and algebraic operations yield

$$\begin{aligned} v_{L_{av}}(kT_s) &= \frac{2\sin(\pi f_m T_s)}{T_s}\sin(2\pi f_m k T_s + \pi f_m T_s) \\ &\quad - \frac{\sin(\pi f_m T_s)}{T_s}\sin(2\pi f_m k T_s + \pi f_m T_s) \\ &\quad - \frac{\sin(\pi f_m T_s)}{T_s}\sin(2\pi f_m k T_s + \pi f_m T_s) = 0. \end{aligned} \tag{27}$$

Note that the sampling was performed at $t = kT_s$, i.e., for $\tau = 0$. A different τ value, for example $\tau = T_s/2$, will lead to totally different results.

SAM BEN-YAAKOV
DOV WULICH
Department of Electrical and Computer Engineering
Ben-Gurion University of the Negev
Beer-Sheva, Israel

[1]Such signals are named "raised cosine".

REFERENCES

[1] Vorperian, V. (1990)
Simplified analysis of PWM converters using the model of the PWM switch: Parts I and II.
IEEE Transactions on Aerospace and Electronic Systems, **26**, 3 (May 1990), 490–505.

[2] Maksimovic', D., and C'uk, S. (1991)
A unified analysis of PWM converters in discontinuous modes.
IEEE Transaction on Power Electronics, **6**, 3 (July 1991).

[3] C'uk, S., and Middlebrook, R. D. (1977)
A general unified approach to modelling switching dc-to-dc converters in discontinuous conduction mode.
IEEE Power Electronics Specialists Conference Record, 1977, pp. 36–57; IEEE Publication 77 CH 12-13-8AES.

[4] Chetty, P. R. K. (1982)
Current injected equivalent circuit approach to modeling of switching dc-dc converters in discontinuous inductor conduction mode.
IEEE Transactions on Industrial Electronics, **IE-29**, 3 (Aug. 1982), 230–234.

[5] Smedley, K. S., and C'uk, S. (1990)
One cycle control of switching converters.
IEEE Power Electronics Specialists Conference Record, 1990, pp. 888–896; IEEE Publication 91CH3008-0.

[6] C'uk, S. (1976)
Modelling, analysis, and design of switching converters.
Ph.D. dissertation, California Institute of Technology, Pasadena, Nov. 1976.

[7] Middlebrook, R. D., and C'uk, S. (1976)
A general unified approach to modelling switching converter power stages.
IEEE Power Electronics Specialists Conference Record, 1976, pp.18–34; IEEE Publication 76 CHO 1084-3AES.

[8] Krien, P. T., Bentsman, J., Bass, R. M., and Lesieutre, B. C. (1990)
On the use of averaging for the analysis of power electronic systems.
IEEE Transactions on Power Electronics, **5**, 2 (Apr. 1990), 182–190.

[9] Sanders, S. R., Noworolski, J. M., Liu, X. Z., and Verghese, G. C. (1991)
Generalized averaging method for power conversion circuits.
IEEE Transactions on Power Electronics, **6**, 2 (Apr. 1991).

WILLIAM M. POLIVKA
IBM Federal Systems Company
Owego, NY

Power Lines: Radar Measurements and Detection Algorithm for Polarimetric SAR Images

Polarimetric radar backscattering measurements of a variety of powerline cables are presented. The objective of the first part of the investigation was to study the effect of braiding of the cables on the backscattering at skew incidence. The measurements were performed for four different actual size powerline samples at C-, X-, and Ka-band over a wide range of incidence angles. The data were collected over a 500 MHz bandwidth at C- and X- band with a 1.25 MHz increment and a 1 GHz bandwidth at Ka-band with a 2.5 MHz increment. Also the effect of nonuniform illumination and measurement in the near field of the cables were studied. Experimental data shows a significant radar backscatter for VV-polarization (σ_{vv}) at angles away from normal incidence. This backscatter is proportional to the number and diameter of the strands on the surface of the cables. There is also noticeable backscatter for the HH and VH components of the scattering matrices. Their magnitudes, relative to that of the VV component, are proportional to the pitch angle of the helix.

Since detection of these cables is an important safety issue for low-flying airplanes a detection algorithm using polarimetric synthetic aperture radar (SAR) images was developed using the knowledge gleaned from the measurements.

The detection algorithm was tested on a simulated image and worked well, detecting a power line whose backscatter power was 6 dB below the average background power.

I. INTRODUCTION

Detection and collision avoidance of obstacles of small physical cross section has always been an important problem for low-flying aircrafts. High voltage powerlines and powerline towers are particularly hazardous in this respect.

Many collision warning techniques have been suggested in the past. Among the most promising techniques are laser radar [Savan and Barr, 1988] and millimeter wave radar [Rembold et al., 1982], particularly the latter when used in the synthetic aperture imaging mode. Available methods, however, suffer from a number of shortcomings. A major limitation of laser systems is atmospheric attenuation under fog and cloudy conditions, which would hamper

Manuscript received February 19, 1993; revised May 28 and August 23, 1993.

IEEE Log No. T-AES/30/2/15832.

This research was performed under subcontract to Ressler Associates, Inc., under DARPA/SBIR contract number DAAH01-91-C-R066.